Supplementary Information:

Tailoring Phonon Polaritons in hBN with the Plasmonic Phase-Change Material In_3SbTe_2

Author(s) and Corresponding Author(s)*:

Lina Jäckering*,+,1, Aaron Moos+,1, Lukas Conrads[1], Yiheng Li[1], Alexander Rothstein[2,3], Dominique Malik[1], Kenji Watanabe[4], Takashi Taniguchi[5], Matthias Wuttig[1,6,7], Christoph Stampfer[2,3,7], Thomas Taubner*,1

*jaeckering@physik.rwth-aachen.de; taubner@physik.rwth-aachen.de

+both authors contributed equally

Affiliations

[1]1st Institute of Physics (IA), RWTH Aachen University, 52074 Aachen, Germany

[2]2nd Institute of Physics, RWTH Aachen University, 52074 Aachen, Germany

[3]Peter Grünberg Institut (PGI-9), Forschungszentrum Jülich, 52425 Jülich, Germany

[4]Research Center for Electronic and Optical Materials, National Institute for Materials Science, 1-1 Namiki, Tsukuba 305-0044, Japan

[5]International Center for Materials Nanoarchitectonics, National Institute for Materials Science, 1-1 Namiki, Tsukuba 305-0044, Japan

[6] Peter Grünberg Institut (PGI-10), Forschungszentrum Jülich, 52425 Jülich, Germany

[7]Juelich-Aachen Research Alliance (JARA-FIT), 52425 Juelich, Germany

This PDF file includes:

Methods

Supplementary Note 1: Fast prototyping of resonators written into IST below hBN flakes of various thicknesses

Supplementary Note 2: Hyperbolic phonon polaritons

Supplementary Note 3: Dispersion of hyperbolic phonon polaritons in hBN on amorphous and crystalline IST

Supplementary Note 4: Analysis of the quality factor of an optically programmed resonator into IST below hBN

Supplementary Note 5: Simulation of reconfigurable focusing of polaritons in hBN by a launching arc structure

Supplementary Note 6: Comparative study of reconfigurable polariton optics and polariton resonators

References

Methods

Sample Fabrication. Using direct current and radio frequency sputter deposition, a 50 nm thick layer of amorphous In_3SbTe_2 and a 20 nm thick capping layer of $ZnS:SiO_2$ were applied on a Si substrate. The capping layer (80% ZnS, 20% SiO_2) prevents the sample from oxidation. Flakes of hBN were then directly exfoliated onto the previously described amorphous PCM sample.

Optical switching. A home-built laser switching setup was used to crystallize the PCM locally. Here, the light of a 660 nm laser diode is focused on the sample with a 10-fold objective with NA = 0.25. Each individual crystallized spot for the resonator structures was created by applying 100 pulses with a power of 91 mW and a pulse length of 800 ns. Due to the elliptical beam profiles the crystallized spots are elliptical. One elliptical crystallized spot has a lateral extension of approximately 1 x 1.5 μm^2. The sample was placed on a Thorlabs piezo stage (Thorlabs MAX311D/M with BPC303 piezo controller) allowing for precise movements of the sample. The amorphous resonator is created by placing multiple crystalline spots next to each other and leaving out a circular amorphous region in the center, the resonator. As the hBN flake we used to investigate the launching arc structures is thicker, we slightly adapted the parameters for laser crystallization. In case of the arc structures, the individual crystallized spots were created by applying 100 pulses with a power of 103 mW and a pulse length of 900 ns. Again, the structures were created by placing multiple spots next to each other.

s-SNOM. We used a commercially available s-SNOM (NeaSNOM neaspec GmbH) to image the polaritons in hBN on IST. We combined commercially available quantum cascade lasers (MIRcat-QT Mid-IR Laser and QCL by DRS Daylight Solutions) with a liquid nitrogen-cooled Mercury Cadmium Tellurium detector to investigate polaritons in the wavenumber range from 1390 to 1600 cm^{-1}. We used the pseudoheterodyne detection scheme to obtain s-SNOM amplitude and phase. We performed our measurements using tapping amplitudes between 65 and 75 nm and demodulated the signal at the second demodulation order.

Numerical Field Simulations. Numerical simulations were performed with the commercial solver CST Studio Suite from Dassault Systèmes. The simulation was modelled with Floquet port excitation using an incident angle of the p-polarized light of 60° normal to the surface and unit cell boundary conditions in lateral and open boundary conditions in vertical dimensions.

The constant loss-free refractive index of 3.4 was used for Si. The dielectric function of IST is shown Figure 1a. A constant refractive index of 2.1 was assumed for the $ZnS:SiO_2$. The anisotropic dielectric function of hBN was modelled according to Figure 2b.

The electric field was extracted 1 nm above the sample surface. The fields were normalized with respect to the incident field. Cross-section fields were calculated normal to the p-polarized light in the center of the resonator structure.

Effects of the SNOM tip were not considered in our simulations.

Supplementary Note 1: Fast prototyping of resonators written into IST below hBN flakes of various thicknesses

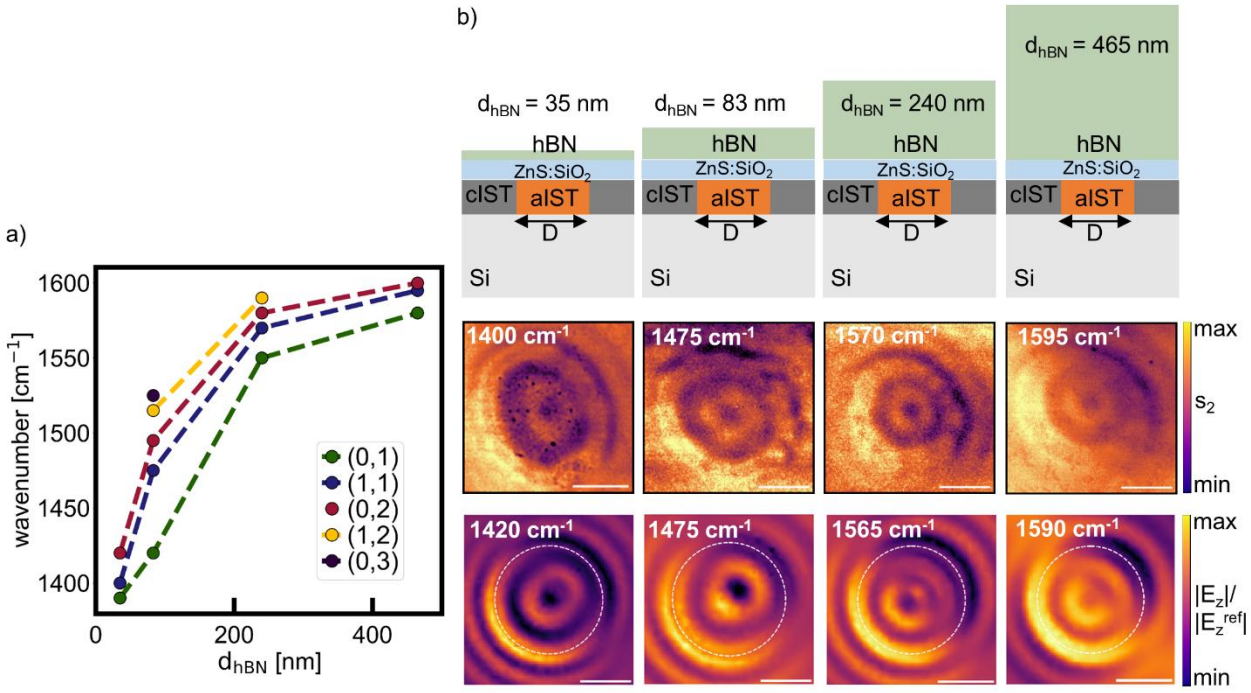


Figure S1: Fast prototyping of resonators written into IST below hBN flakes of various thicknesses. *a) Estimated resonant wavenumber of various resonator modes for different hBN thicknesses. b) s-SNOM amplitude images (top) and electric field simulations (bottom) of the (1,1) mode (blue in a)) for four different hBN thicknesses. The scale bars correspond to 1 µm.*

Exploiting the fast prototyping we program amorphous resonators (D ~ 2µm) into IST below hBN flakes of four different thicknesses ranging from 35 to 465 nm. Sequential s-SNOM spectroscopy of the resonator modes allows us to identify the mode evolution with photon wavenumber for the different hBN thicknesses as summarized in Figure S1a. For each hBN thickness we can at least identify the (0,1), (1,1) and (0,2) mode (c.f. Figure S2). With increasing hBN thickness the modes are found at higher wavenumbers as expected form the thickness-dependent dispersion of hBN's PhP.[1] Figure S1b illustrates the change of the resonance wavenumber of the (1,1) mode for the different hBN thicknesses showing s-SNOM amplitude images of the mode at the top and corresponding electric field simulations at the bottom.

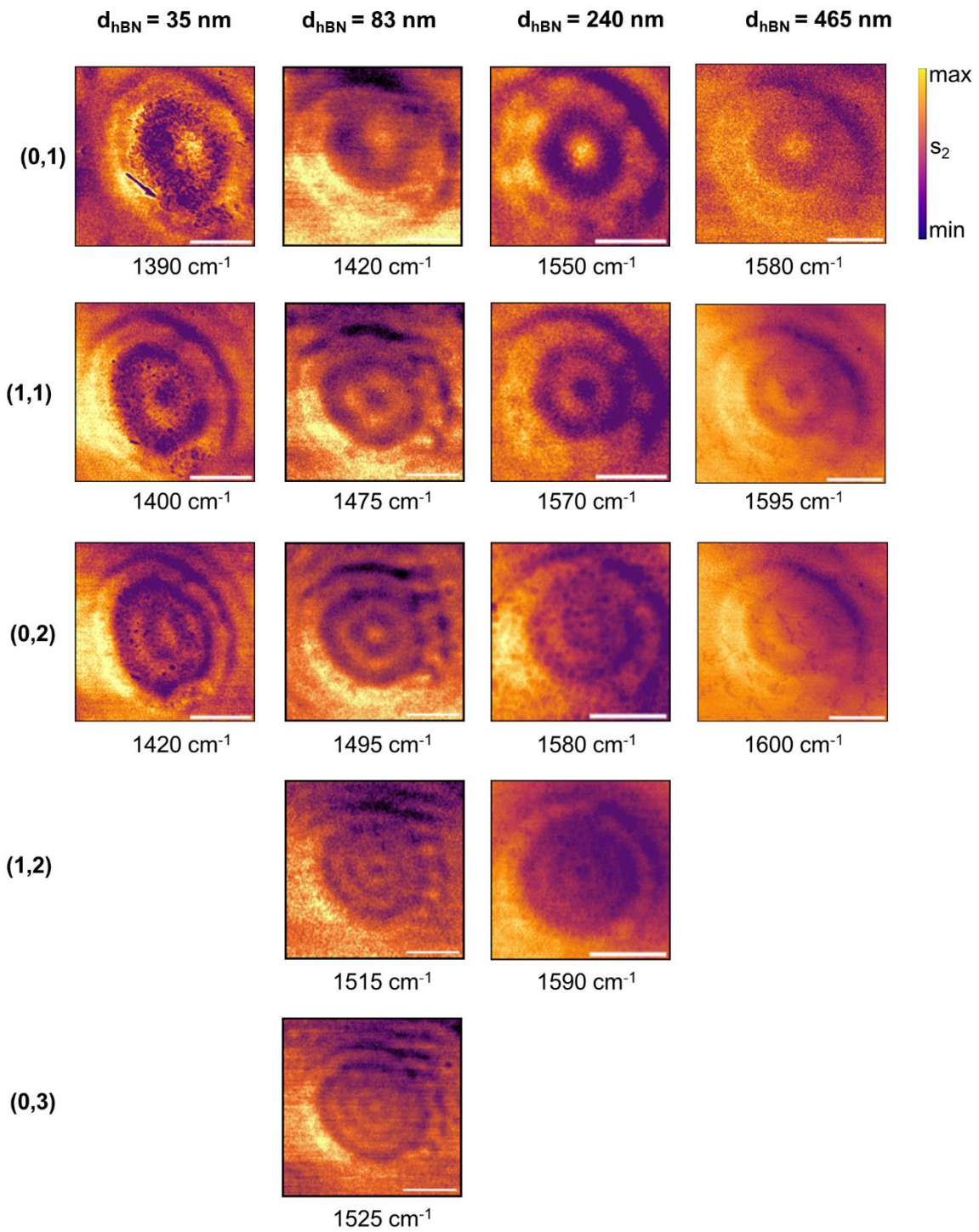


Figure S2: Near-field imaging of higher order resonator modes for various hBN thicknesses. *s-SNOM amplitude images of resonator modes with increasing mode order from top to bottom and for four different hBN thicknesses that increase from left to right. For all hBN thicknesses the resonator diameter is approximately 2 μm. The scale bars correspond to 1 μm.*

Supplementary Note 2: Hyperbolic Phonon Polaritons

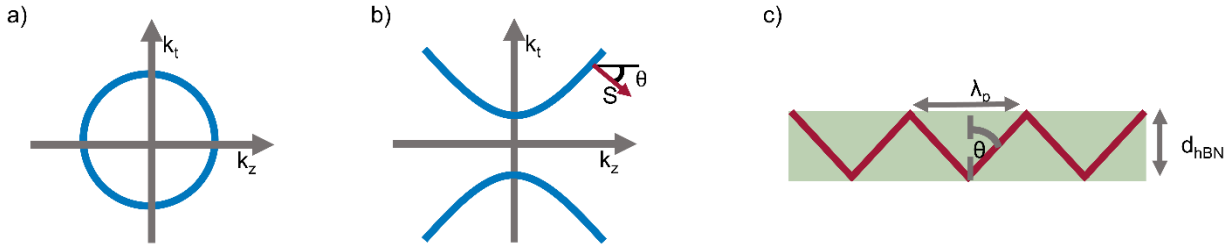


Figure S3: Hyperbolic phonon polaritons in hBN. *a) Isofrequency curve of an isotropic medium. b) Isofrequency curve of a hyperbolic medium. c) Sketch of the HPhP propagation through an hBN slab.*

In isotropic media, the permittivity is the same along all directions and therefore polaritons propagate uniformly in all directions. The uniform propagation behavior is visualized in the isofrequency curve in Figure S3a. For a given photon frequency, the magnitude of the polariton wavevector is fixed whereas the propagation direction is free.

In contrast to isotropic media, hyperbolic media have distinct permittivities along the different optical axes which are opposite in sign.[2] From the dispersion relation, we obtain hyperbolic shaped isofrequency curves as depicted in Figure S3b. For a given photon frequency, the magnitude of the polariton wavevector is not fixed as for isotropic media but can—in principle—be infinitely large. The propagation direction, however, is fixed for a given photon frequency for large wavevectors. The propagation angle can be approximated by $\tan\theta(\nu) = i\frac{\sqrt{\varepsilon_t(\nu)}}{\sqrt{\varepsilon_z(\nu)}}$.[3,4]

Consequently, inside the hBN slab the HPhPs propagate under the angle $\theta(\nu)$ as it is sketched in Figure S3c. The HPhPs propagate through the slab and are reflected at the interfaces forming volume-confined modes. The polariton wavelength corresponding to the spacing of the periodic field pattern at the hBN surface can be derived from the geometry: $\lambda_p = 2\, d_{hBN}\ tan\ \theta(\nu)$.[3] When the actual layer stack rather than a free-standing hBN slab is considered, factors such as the reflection phase at the material interface need to be accounted for. Thus, the polariton wavelength will deviate from the simple geometric description.[3]

Supplementary Note 3: Dispersion of Hyperbolic Phonon Polaritons in hBN on amorphous and crystalline IST

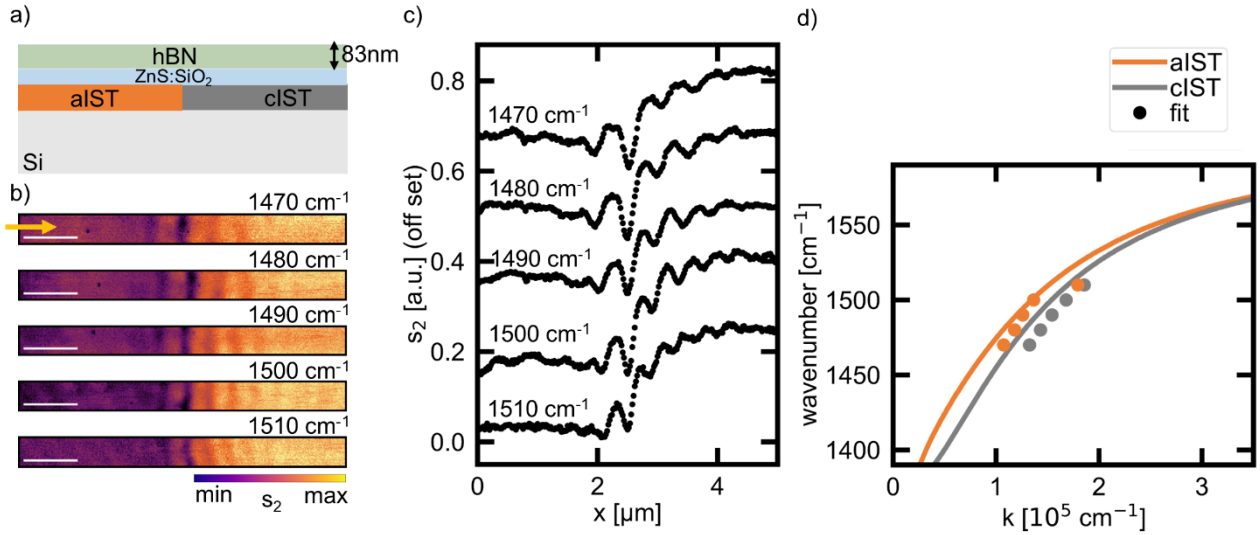


Figure S4: Dispersion of HPhPs in hBN on aIST and cIST*. a) Sketch of the phase boundary with hBN on aIST marked in orange on the left and on cIST marked in grey on the right at that polaritons are launched towards both sides. b) s-SNOM amplitude images of polaritons launched at the phase boundary for five different wavenumbers. The yellow arrow indicates the illumination direction. The scale bars correspond to 1 µm. c) Line profiles extracted from the s-SNOM amplitude images shown in b). d) Experimental (dots) and calculated (solid lines) dispersion of the HPhPs in hBN on cIST in grey and on aIST in orange.*

Here, we experimentally show (i) that the propagation behavior of the HPhPs in hBN can be altered when switching the amorphous IST below the hBN (on the left in sketch in Figure S4a) to crystalline IST (on the right in sketch in Figure S4a) and (ii) that the phase boundary can act as polaritons launcher. Accordingly, we performed s-SNOM amplitude images of phonon polaritons in hBN launched at an IST phase boundary below (Figure S4b). We extracted line profiles from the s-SNOM amplitude images (Figure S4c) which show pronounced periodic maxima on the crystalline (right) side of the phase boundary and weaker periodic maxima on the amorphous side. The periodic maxima correspond to interference of polaritons launched at the phase boundary that propagate to both sides with the incident light. For HPhP on cIST we estimate the polariton propagation length to be 1-1.5 µm and on aIST to be ~1 µm. We attribute the suppression of polaritons on the amorphous side to shadowing by the s-SNOM tip of the phase boundary that launches the HPhP when scanning on the amorphous side as the illumination is

from the left (marked by yellow arrow) in the shown images. This effect of shadowing by the s-SNOM tip has also been observed for HPhP launched at a flake edge.[5]

From fits to the line profiles, we extracted the polariton wavevector and plotted the experimental dispersion relation together with the theoretical one (Figure S4d). We calculated the theoretical dispersion using the Transfer Matrix Method[6] to determine the reflection coefficient as a function of photon wavenumber and polariton wavevector and then extracted the mode from the imaginary part of the reflection coefficient. Both experimental and theoretical dispersion show an increasing wavevector with increasing photon wavenumbers for hBN on aIST and on cIST. The experimental and theoretical dispersions of the HPhPs in the two layer stacks show that the HPhPs have a larger wavevector (smaller wavelength) when the hBN is on cIST over the whole spectral range. For higher photon wavenumbers the difference between the polariton wavelengths decreases and almost vanishes above 1560 cm^{-1}. We observe larger wavevectors in the experimental dispersion than in the theoretical dispersion for HPhP in hBN on both aIST and cIST. This deviation might be due to slightly different thicknesses and nominal permittivities of hBN, IST and the capping in the actual layer stack.

Our results of a dispersion shifted to higher wavevectors for HPhP in hBN on cIST compared to hBN on aIST is in agreement with the observed dispersion shift for HPhP in $h^{10}BN$ on cIST compared to $h^{10}BN$ on aIST by Lu et al.[7]. The observed propagation length of 1-1.5 µm for HPhP on IST with wavevectors in the range of 1.1-1.9 10^5 cm^{-1} is in good agreement with the propagation length of HPhP in hBN on SiO_2-Si substrate (c.f. Figure 5e in ref.[8]). In the same work, Giles et al.[8] report that significantly longer propagation lengths are observed for HPhP in isotopically enriched $h^{10}BN$ and $h^{11}BN$. For polariton wavevectors above 1 10^5 cm^{-1} the propagation length of HPhP in $h^{10}BN$ is almost twice the propagation length of HPhP in natural abundant hBN. The longer propagation length is attributed to the longer lifetime of HPhP in

isotopically enriched hBN. We expect that HPhP in isotopically enriched hBN on IST will also show longer propagation length.

Supplementary Note 4: Analysis of the quality factor of an optically programmed resonator into IST below hBN

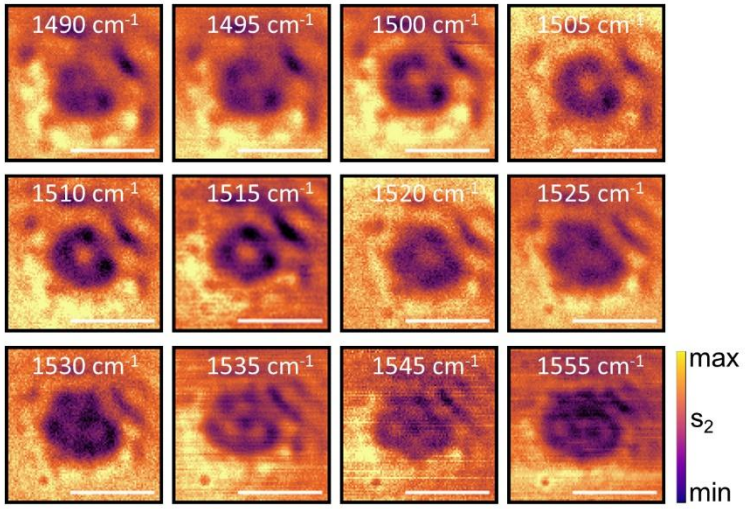


Figure S5: Analysis of the quality factor of an optically programmed resonator into IST for HPhP in hBN. s-SNOM amplitude images of the spectral evolution of the (0,1) mode to the (1,1) and subsequently (0,2) mode of the resonator with a diameter of 0.9 μm programmed into IST below 83 nm thick hBN flake. The scale bars correspond to 1 μm.

To determine the quality factor of optically programmed resonators in IST for HPhP in hBN, we performed sequential s-SNOM spectroscopy of the (0,1) mode of the resonator with a diameter of 0.9 μm (Figure S5a) also discussed in Figure 3. With increasing photon wavenumber, the s-SNOM amplitude inside the cavity evolves from a uniform distribution at 1490 cm^{-1} to a high amplitude in the center with a ring of low amplitude at around 1510 cm^{-1} to a uniformly low amplitude at 1525 cm^{-1}. This evolution is assigned to the spectral evolution of the (0,1) mode. For higher wavenumbers a low amplitude in the center with a ring of high amplitude is observed that evolves into a high amplitude in the center with a ring of low amplitude and a ring of high amplitude around it which we assign to the (1,1) mode at 1545 cm^{-1} evolving into the (0,2) mode at 1555 cm^{-1}.

From the s-SNOM amplitude images we extract the amplitude in the center of the resonator normalized to the amplitude away from the center but inside the resonator. The spectral evolution of the normalized s-SNOM amplitude is shown in Figure 3d.

Supplementary Note 5: Simulation of reconfigurable focusing of polaritons in hBN by a launching arc structure

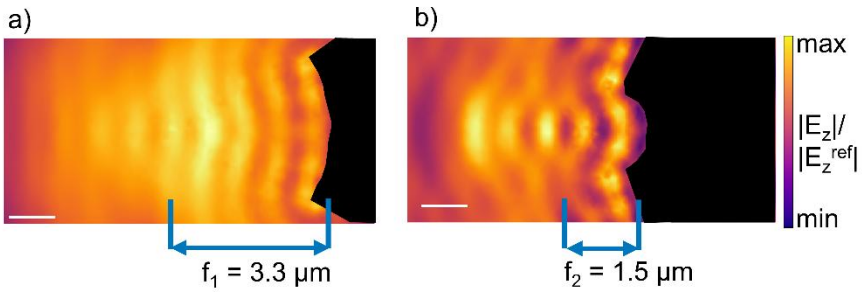


Figure S6: Simulation of reconfigurable focusing of polaritons in hBN by a launching arc structure*. a) Electric field simulation at 1480 cm^{-1} of hBN's HPhPs launched and focused to 3.3 µm by the launching arc structure. b) Electric field simulation at 1480 cm^{-1} of hBN's HPhPs launched and focused to 1.5 µm by the reconfigured launching arc structure. The scale bars correspond to 1 µm.*

To support our experimental results (Figure 4 main text) on the reconfigurable focusing of polaritons in hBN by a launching arc structure optically programmed into IST (discussed in the main text), we performed electrical field simulations. Figure S6a and S6b show the electrical field simulations of a crystalline launching arc structure programmed in the IST below hBN with an inner curvature of 3 µm and the reconfigured structure with an inner curvature of 1 µm, respectively. In the simulation, we observe a focal point of 3.3 µm and 1.5 µm for the arc structure with larger and smaller curvature, respectively, which are larger than the expected focal length of 3 and 1 µm retrieved from the curvature. This deviation probably results from the interference of the polaritons launched by the crystalline arc structure with the incoming light incident from the right. Deviations of the focal length in simulation and experiment might originate from deterioration and inhomogeneities in the shape of the fabricated arc structure.

Supplementary Note 6: Comparative study of reconfigurable polariton optics and polariton resonators

Publi-cation	Pola-riton-hosting material	Tuning mechanism	Free propagation	Nanostructures	mode ana-lysis	Confine-ment quality factor
This work	hBN (nat. abund.)	Phase change in IST - Non-volatile - Reconfigurable - Modification of size and shape	**Launching** at phase boundary	Circular **resonator** **Launching focusing** structure	Yes, up to (0,3)	λ/39 Q~72
Folland et al. [9]	$h^{10}BN$	Phase transition in vanadium dioxide - volatile	**Launching** at phase boundary **Refraction** across phase boundary	Theoretical modeling of metasurface (far-field), lens and waveguide	-	-
Lu et al. [7]	$h^{10}BN$ α-MoO_3	Phase change in IST - Non-volatile - Reconfigurable	Free propagation of HPhP in hBN and α-MoO3 tailored by IST phases	**launching and focussing** antenna for HPhP in α-MoO3	-	-
Chau-dhary et al. [10]	$h^{11}BN$	Phase change in GST - Non-volatile - Reconfigurable		**Refractive** lens, prism, metalens, waveguide	-	-
Agha-miri et al. [11]	$h^{10}BN$ α-MoO_3	Tune charge carrier concentration in $SmNiO_3$ (SNO) via - strong local fields: non-volatile - hydrogenation: non-volatile, global - temperature: volatile, global	Free propagation of HPhP in hBN and α-MoO_3 tailored by tuned local conductivity in SNO;	Triangular **cavity** for HPhP in hBN (not reconfigure nor tailored) Circular, rectangular **resonator** for HPhP in α-MoO_3 (not reconfigured nor tailored)	-	-
Duan et al.[12]	$h^{10}BN$	No tuning $h^{10}BN$ on graphene: Tuning of fermi energy in graphene - volatile		Rectangular **resonators**	Yes	λ/43 Q~165 Q~75.9
Tamag-none et al.[13]	$h^{11}BN$ α-MoO_3	No tuning		Circular **resonators**	Yes	Q~332 Q~250
Shein-fux et al.[14]	$h^{11}BN$	No tuning		Rectangular **resonators**	Yes	Q~50-90 (d_{hBN}=25-33 nm) Q~100-480 (d_{hBN}=3 nm)

Sumi-kura et al.[15]	SiC	Phase change in GST - Non-volatile - Turn on and off		Circular **resonator**	yes	λ/50 -
Li et al.[16]	quartz	Phase change in GST - Non-volatile - Write and erase	**Launching** at phase boundary	Circular **resonator**	yes	λ/80 Q~95
Con-rads et al. [17]	SiC	Phase change in IST - Non-volatile - Reconfigurable - Modification of shapes	**Launching** at phase boundary	Circular, rectangular, triangular **resonators**	yes	λ/35 Q~50

Table S1: Comparative study of reconfigurable polariton optics and polariton resonators

We performed a comparative study of hBN polariton resonators and reconfigurable polariton optics with related literature published previously to highlight the novelty of reconfigurable resonators demonstrated in this work and to compare the performance of those resonators. We evaluated the tuning mechanism, tunability, confinement and quality factor (see Table S1).

Comparison to previously investigated tunable or reconfigurable polariton optics

Our work adds a significant step towards fast-prototyping of reconfigurable polariton optics for vdWM. Folland et al.[9] introduced the volatile phase transition material vanadium dioxide (VO_2) to polariton optics with vdWM in 2018 and showed launching at and refraction across a phase boundary. Notably, the creation of nanostructures with VO_2 would still need to rely on cumbersome nanofabrication techniques as either the VO_2 would need to be patterned or its phase transition properties locally modified. Chaudhary et al.[10] caught up on their theoretical suggestion of a lens for HPhP and programmed it into the PCM GST. Chaudhary et al. restricted their work to refractive polariton optics with GST—investigating refraction of HPhPs launched at the hBN edge across local structures programmed into GST. In contrast, Aghamiri et al.[11] introduced the oxide SNO, whose conductivity can be tuned and thereby its optical properties, to program nanophotonic devices relying on reflection. Although Aghamiri et al. demonstrated reconfigurability with their material system and the capability to program resonators for vdWM,

they did not systematically study the performance of such a resonator nor demonstrated its reconfigurability. In this work, we employ the PCM IST to demonstrate fast-prototyping of resonators for HPhP in hBN and reconfiguring the resonator size. Further, we determine the performance by measures of confinement (λ/39) and quality factor (Q~72).

Comparison to previously investigated reconfigurable resonators for bulk polariton-hosting materials

Our choice of IST was inspired by the journey of reconfigurable polariton optics for bulk polariton-hosting materials. Similarly, in the beginning the well-known PCM GST has been used for reconfigurable polariton optics. Li et al.[16] and Sumikura et al.[15] demonstrated writing and erasing of resonators for PhP in quartz, and turning on and off resonances of conventionally fabricated resonators for PhP in SiC with GST, respectively. Conrads et al. exploited the PCM IST to reconfigure size and shape of resonators for PhPs in SiC[17] and surface plasmon polaritons in CdO[18].

Comparison to previously investigated conventionally fabricated resonators for hyperbolic phonon polaritons in hBN

Finally, we compare the performance of our reconfigurable resonators for HPhP in hBN programmed into IST (confinement (λ/39) and quality factor (Q~72)) to conventionally fabricated HPhP resonators. Fabricating resonators with ultra-high quality factors up to Q = 480 has been shown by Sheinfux et al.[14] demonstrating the capabilities of hBN resonators. Resonators showing these ulta-high quality factors required tremendous fabrication efforts as they created only 600 nm x 600 nm holes into a gold film and then aligned an $h^{11}BN$ flake of only 3 nm thickness onto the holes. Similarly fabricated very small resonators (width down to 50 nm cavity

width) for thicker $h^{11}BN$ flakes (25 and 33 nm) did only show quality factors up to 40-125, which are comparable (or slightly higher) to the quality factor of 72 we observed. These results by Sheinfux et al. suggest that a thinner $h^{11}BN$ flake enables higher quality factors, also applicable for our approach. Duan et al.[12] and Tamagnone et al.[13] instead fabricated hBN resonators ($h^{10}BN$ and $h^{11}BN$, respectively) by etching away the hBN flake leaving only the resonator. The resonators by Duan et al. have similar geometries (2.7 µm x 2.7 µm; d_{hBN}=73 nm) like ours and a comparable confinement but a higher quality factor whereas Tamagnone et al. investigated smaller resonators for comparable thick flakes (D = 70 nm; d_{hBN}=70 nm) and observed quality factors of 332 exceeding the quality factor obtained in this work, implying that a smaller resonator leads to higher quality factors.

By placing the $h^{10}BN$ resonator (of same geometry) onto graphene whose Fermi-Energy can be tuned by applying a gate-voltage Duan et al.[12] also created a tunable resonator. This tunable resonator showed a quality factor of Q~75.9 comparable to our results of Q~72.

Remarkably, in contrast to our work that used naturally abundant hBN, the mentioned previous studies on resonators for HPhP in hBN did use isotopically enriched hBN ($h^{10}BN$ or $h^{11}BN$). HPhP in isotopically enriched hBN have longer propagation lengths due to longer lifetimes.[8] We expect that the longer propagation length implies a higher quality factor, however we could not find a comparative study of resonators for different hBN isotopes. Therefore, we assume the quality factor of reconfigurable resonators programmed into IST could be further improved by using isotopically enriched hBN.

Summing up, with fast-prototyping using IST we created a reconfigurable resonator for HPhP in hBN that does show a similar quality factor to previously investigated conventionally fabricated tunable resonators although we used natural abundant hBN. Compared to static resonators for HPhPs in isotopically enriched hBN the resonators in this work showed comparable confinement but quality factors that were much lower especially to the highest reported values for resonators

for very thin flakes or of much smaller size. We expect that also with optically programmed resonators in IST higher quality factors could be achieved when using isotopically enriched hBN, thinner hBN flakes and creating smaller resonators.

References

1. Dai, S. *et al.* Tunable phonon polaritons in atomically thin van der Waals crystals of boron nitride. *Science* **343,** 1125–1129; 10.1126/science.1246833 (2014).

2. Caldwell, J. D. *et al.* Photonics with hexagonal boron nitride. *Nat Rev Mater* **4,** 552–567; 10.1038/s41578-019-0124-1 (2019).

3. Dai, S. *et al.* Subdiffractional focusing and guiding of polaritonic rays in a natural hyperbolic material. *Nature communications* **6,** 6963; 10.1038/ncomms7963 (2015).

4. Li, P. *et al.* Hyperbolic phonon-polaritons in boron nitride for near-field optical imaging and focusing. *Nature communications* **6,** 7507; 10.1038/ncomms8507 (2015).

5. Dai, S. *et al.* Efficiency of Launching Highly Confined Polaritons by Infrared Light Incident on a Hyperbolic Material. *Nano letters* **17,** 5285–5290; 10.1021/acs.nanolett.7b01587 (2017).

6. Zhan, T., Shi, X., Dai, Y., Liu, X. & Zi, J. Transfer matrix method for optics in graphene layers. *Journal of Physics: Condensed Matter* **25,** 215301; 10.1088/0953-8984/25/21/215301 (2013).

7. Lu, D. *et al.* Tunable hyperbolic polaritons with plasmonic phase-change material In 3 SbTe 2. *Nanophotonics* **13,** 937–944; 10.1515/nanoph-2023-0911 (2024).

8. Giles, A. J. *et al.* Ultralow-loss polaritons in isotopically pure boron nitride. *Nature materials* **17,** 134–139; 10.1038/nmat5047 (2018).

9. Folland, T. G. *et al.* Reconfigurable infrared hyperbolic metasurfaces using phase change materials. *Nature communications* **9,** 4371; 10.1038/s41467-018-06858-y (2018).

10. Chaudhary, K. *et al.* Polariton nanophotonics using phase-change materials. *Nature communications* **10,** 4487; 10.1038/s41467-019-12439-4 (2019).

11. Aghamiri, N. A. *et al.* Reconfigurable hyperbolic polaritonics with correlated oxide metasurfaces. *Nature communications* **13,** 4511; 10.1038/s41467-022-32287-z (2022).

12. Duan, J. *et al.* Active and Passive Tuning of Ultranarrow Resonances in Polaritonic Nanoantennas. *Advanced Materials* **34,** e2104954; 10.1002/adma.202104954 (2022).

13. Tamagnone, M. *et al.* High quality factor polariton resonators using van der Waals materials. *arXiv*. October 1, 2020; 10.48550/arXiv.1905.02177v2 (accessed 2025-03-04).

14. Herzig Sheinfux, H. *et al.* High-quality nanocavities through multimodal confinement of hyperbolic polaritons in hexagonal boron nitride. *Nature materials* **23,** 499–505; 10.1038/s41563-023-01785-w (2024).

15. Sumikura, H. *et al.* Highly Confined and Switchable Mid-Infrared Surface Phonon Polariton Resonances of Planar Circular Cavities with a Phase Change Material. *Nano letters* **19,** 2549–2554; 10.1021/acs.nanolett.9b00304 (2019).

16. Li, P. *et al.* Reversible optical switching of highly confined phonon-polaritons with an ultrathin phase-change material. *Nature materials* **15,** 870–875; 10.1038/nmat4649 (2016).

17. Conrads, L., Schüler, L., Wirth, K. G., Wuttig, M. & Taubner, T. Direct programming of confined surface phonon polariton resonators with the plasmonic phase-change material In3SbTe2. *Nat Commun* **15,** 3472; 10.1038/s41467-024-47841-0 (2024).

18. Conrads, L. *et al.* Real-space imaging of confined infrared surface plasmon polaritons on doped semiconductors covered with phase-change materials. *Science advances* **11,** eadr6844; 10.1126/sciadv.adr6844 (2025).